Turbulent kinetic energy spectra of solar convection from New Solar Telescope observations

and realistic magnetohydrodynamic simulations

Turbulent kinetic energy spectra of solar convection from New Solar Telescope observations and realistic magnetohydrodynamic simulations

I N Kitiashvili[1,2,3]**, V I Abramenko**[4]**, P R Goode**[4]**, A G Kosovichev**[1]**,
S K Lele**[2,5]**, N N Mansour**[6]**, A A Wray**[6]** and V B Yurchyshyn**[4]

[1] W W Hansen Experimental Physics Laboratory, Stanford University, Stanford, CA 94305, USA
[2] Center for Turbulence Research, Stanford University, Stanford, CA 94305, USA
[3] Kazan Federal University, Kazan 420008, Russia
[4] Big Bear Solar Observatory of New Jersey Institute of Technology, CA 40386, USA
[5] Aeronautics and Astronautics Department, Stanford University, Stanford, CA 94305, USA
[6] NASA Ames Research Center, Moffett Field, CA 94035, USA

E-mail: irinasun@stanford.edu

Abstract
Turbulent properties of the quiet Sun represent the basic state of surface conditions and a background for various processes of solar activity. Therefore, understanding the properties and dynamics of this 'basic' state is important for the investigation of more complex phenomena, the formation and development of observed phenomena in the photosphere and atmosphere. For the characterization of turbulent properties, we compare the kinetic energy spectra on granular and sub-granular scales obtained from infrared TiO observations with the New Solar Telescope (Big Bear Solar Observatory) and from three-dimensional radiative magnetohydrodynamic (MHD) numerical simulations ('SolarBox' code). We find that the numerical simulations require high spatial resolution with a 10–25 km grid step in order to reproduce the inertial (Kolmogorov) turbulence range. The observational data require an averaging procedure to remove noise and potential instrumental artifacts. The resulting kinetic energy spectra reveal good agreement between the simulations and the observations, opening up new perspectives for detailed joint analyses of more complex turbulent phenomena on the Sun and possibly on other stars. In addition, using the simulations and observations, we investigate the effects of a background magnetic field, which is concentrated in self-organized complicated structures in intergranular lanes, and observe an increase of the small-scale turbulence energy and its decrease at larger scales due to magnetic field effects.

PACS numbers: 96.60.−j, 96.60.Mz, 96.50.Tf, 95.30.Qd, 47.27.ep

(Some figures may appear in color only in the online journal)

1. Introduction

Understanding and characterization of turbulent solar convection is a key problem of heliophysics and astrophysics. The solar turbulence driven by convective energy transport determines the dynamical state of the solar plasma and leads to excitation of acoustic waves [14], formation of magnetic structures [6, 13] and other dynamical phenomena. Realistic numerical simulations of solar magnetoconvection are an important tool for understanding many observed phenomena, verification and validation of theoretical models and interpretations of observations. Simulations of this type were started in pioneering works of Stein and Nordlund [26] with the main idea of constructing numerical models based
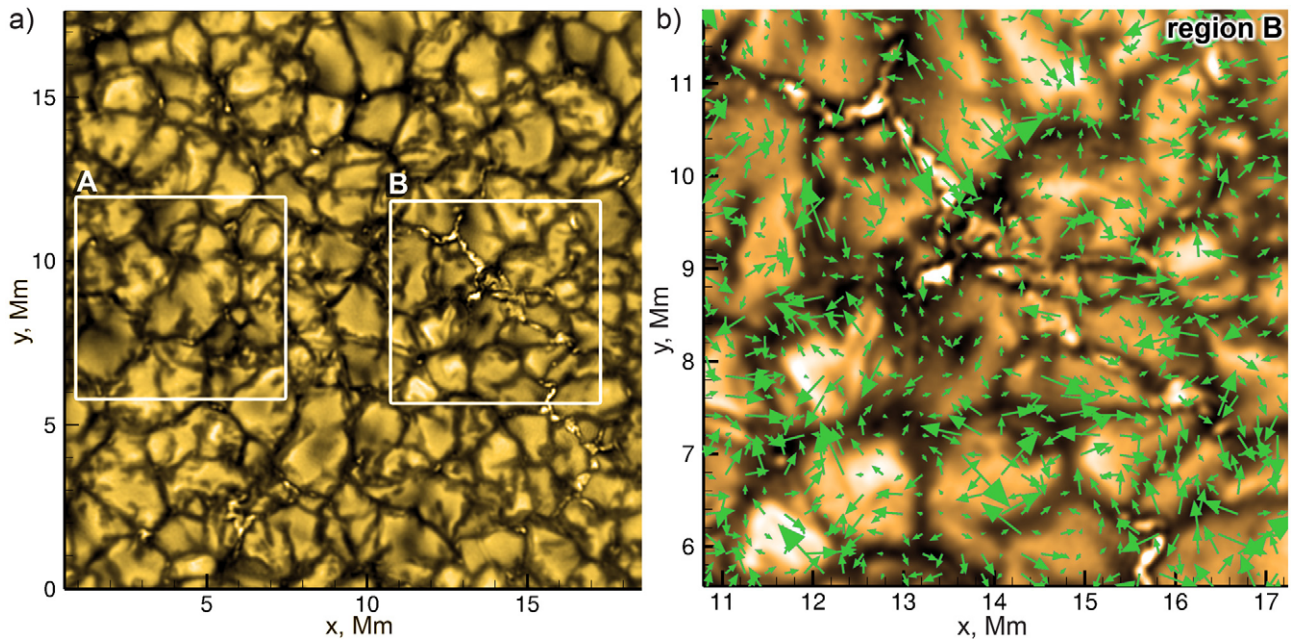
1

Figure 1. A quiet-Sun region observed in the TiO filter with the NST on 3 August 2010. Squares in panel (a) show two subregions: subregion A without magnetic bright points and subregion B with conglomerates of magnetic bright points concentrated in the intergranular lanes. In panel (b), subregion B is shown in detail with overplotted velocity field derived by an LCT method.

on first physical principles. The 'quiet Sun' describes a background state of the solar surface layers without sunspots and active regions, that is, without large-scale magnetic flux emergence and other strong magnetic field effects, which can significantly change properties of the turbulent convection. Quiet-Sun regions are characterized by a weak mean magnetic field of 1–10 G, which is usually concentrated in small-scale flux tubes in the intergranular lanes. The flux tubes are observed as bright points in molecular absorption lines. Previous investigations on the solar turbulent spectra from observations were reported by Abramenko *et al* [1], Goode *et al* [10], Matsumoto and Kitai [18], Rieutord *et al* [22], Stenflo [27] and others. The comparison of observations with numerical simulation data initially done by Stein and Nordlund [26] revealed good agreement between correlation power spectra obtained from smoothed simulation data and high-resolution observations from La Palma. Such a comparison of the results of realistic-type magnetohydrodynamic (MHD) modeling with high-resolution observations gives us an effective method for understanding observed phenomena. Recently, advanced computational capabilities made it possible to construct numerical models of solar turbulent convection with a high level of realism. On the other hand, modern high-resolution observational instruments with adaptive optics, such as the 1.6 m New Solar Telescope (NST) at the Big Bear Solar Observatory (BBSO) [11], have allowed us to capture the small-scale dynamics of surface turbulence [3, 10, 30].

In this paper, we compare the turbulent kinetic energy spectra from observed and simulated data sets for the conditions of quiet-Sun regions, and investigate the properties of solar turbulence and background magnetic field effects. We use two types of data: (i) high-resolution observations of horizontal flows from the NST at the BBSO

(NST/BBSO; [10]) and (ii) high-resolution three-dimensional (3D) radiative MHD and hydrodynamic simulations [15].

2. Observational data

For comparison, we use the broadband TiO filter (centered at 7057 Å) data of a quiet-Sun region obtained with the NST/BBSO [11] on 3 August 2010. The telescope has a 1.6 m aperture (with an off-axis design) and an adaptive optics system, implementing a speckle image reconstruction [29], which allows us to achieve the diffraction-limited resolution of $\sim$77 km in this spectral range. The image sampling is $0.0375''$ ($\sim$27 km) per pixel. The unprecedented spatial resolution together with the high temporal resolution, 10 s, allows us to resolve and investigate the structure and dynamics of very tiny structures on the Sun, such as jet-like structures on the scale of a granule or less [10], and substructures of granules [30], the dynamics of magnetic bright points [2, 17] and the turbulent diffusion properties of solar convection [3].

The analyzed data set of the quiet-Sun region with a size of $28.2'' \times 26.2''$ includes a 2 h time sequence of TiO images with 10 s cadence. To investigate how the magnetic field affects the turbulent properties, we select two subregions, marked as A and B in figure 1(a). Region A has almost no magnetic bright points (BPs), whereas region B includes conglomerates of BPs, which represent concentrations of the magnetic field. A correlation between BPs and magnetic field structures was previously discussed by Berger and Title [5]. For the reconstruction of the horizontal velocity field from the observations, a local correlation tracking (LCT) method [21, 28] was used. Figure 1(b) shows an example of the velocity field plotted over the corresponding TiO intensity image for region B. Calculations of the energy spectra for both

the observational and simulation data sets were performed by using the same code adopted in [1].

3. Numerical simulations

3.1. Radiative MHD code and computational setup

For the modeling, we use a 3D radiative MHD code ('SolarBox') developed for realistic simulations of the top layers of the convective zone and lower atmosphere [12]. The code takes into account the realistic equation of state, ionization and excitation of all abundant species. Radiative energy transfer between fluid elements is calculated with a 3D multi-spectral bin method, assuming local thermodynamic equilibrium and using the OPAL opacity tables [24]. Initialization of the simulation runs is done from parameters of a standard model of the solar interior [7]. The sub-grid scale turbulence is modeled using a large-eddy simulation (LES) approach [4, 9]. The simulations in this paper were obtained using a Smagorinsky eddy-viscosity model [25] in which the compressible Reynolds stresses are described by the equations given by Moin *et al* [19] and Jacoutot *et al* [12], with the Smagorinsky coefficients $C_S = C_C = 0.001$.

For the investigation of the magnetic field effects, we impose a 10 G initially uniform vertical magnetic field. This field gets concentrated in compact flux-tube-like structures in the intergranular lanes and mimics magnetic field in the solar bright points. In all cases, the simulation results were obtained for a computational domain of $6.4 \times 6.4 \times 6.2 \, \text{Mm}^3$, including a 1 Mm high layer of the atmosphere, with a grid spacing of $\Delta x = \Delta y = 12.5 \, \text{km}$ and $\Delta z = 10 \, \text{km}$. The lateral boundary conditions are periodic. The top boundary is open to mass, momentum and energy transfers and also to radiative flux. The bottom boundary is open for radiation and flows and simulates the energy input from the interior of the Sun.

3.2. Effects of the spatial resolution

One critically important issue in the investigation of turbulent properties of convection is limited spatial resolution. In observations, this means not resolving small-scale information. In numerical simulations, unresolved small-scale dynamics can affect the general turbulent properties of convection due to missing physics of turbulent dissipation. The LES models of turbulence effectively increase the Reynolds number and capture, in part, the dynamics on sub-grid scales, thus providing a more realistic representation of turbulent convection. An important requirement for the LES models is resolving all essential scales of convection, including the transition to the inertial (Kolmogorov) range [8].

Figure 2 shows the effect of numerical resolution on the properties of turbulent vertical velocity spectra in our hydrodynamic simulations of solar convection for three cases of horizontal grid spacing: 50, 25 and 12.5 km. It is not surprising that the simulations with higher resolution reveal numerous, inhomogeneously distributed small-scale flow substructures, mostly concentrated at granular edges, and also more complicated dynamics of granules (panels (a)–(c)). The resolution effect is critical from the point of view of the energy cascade, because unresolved substructures may cause redistribution of energy through all scales. For example,

a comparison of the turbulent spectra in the photosphere layer for different resolutions (figure 2(d)) shows faster energy decay for large wavenumbers (small scales) and slightly higher energy density values on larger scales for the low-resolution (50 km) case (blue curve). Such a dependence of the power density slope on the resolution and effect of the energy increase at large scales was previously found by Stein and Nordlund [26]. In the high-resolution simulation spectrum (12.5 km, red curve), the inertial and dissipative subranges, expected from turbulence theories (e.g. [8]), can be identified. Because of the strong density stratification, the spectral properties change with depth below the surface and also change above the surface. The power density spectra for the horizontal resolutions of 12.5 and 25 km (figures 2(e)–(f)) show similar variations in the turbulent properties of convection at different depths. The layers above the solar surface are characterized by smaller total energy and higher spectral energy density slope. These layers are convectively stable, and the turbulence spectrum reflects convective overshooting. The subsurface layers have stronger, more energetic motions, but the energy density slope decreases. In the deeper layers due to the decreasing velocity magnitude the kinetic energy decreases. Also, in the deeper layers the turbulent scales become larger, flows are more homogeneous, and the energy spectra can be described by the Kolmogorov ($-5/3$) power law [16]. The low-resolution simulations (50 km, figure 2(g)) are capable of capturing only the magnitude of the kinetic energy, but unlike the high-resolution simulations they do not show differences of the turbulent dynamics in different layers.

4. Power spectra and data averaging

For the numerically simulated convection (which in this case is modeled from first principles including all the most significant physics contributions), it is important to resolve all essential scales, including the inertial subrange. Once the inertial subrange is resolved it is assumed that the turbulent cascade will continue to the dissipative subrange following the Kolmogorov law scaling. Following Reynolds's idea of separation of turbulent flows into mean and fluctuating parts, we consider smoothly evolving averaged flows [20]. Because the properties of the averaging can affect the resulting power spectra [10], we consider the energy spectra without averaging and with three different types of averaging (table 1), where case 1 represents ensemble time averaging with an overlapping averaging window, and in cases 2 and 3, we divide the whole data set into individual temporal bins, 2 and 5 min long.

Figure 3 shows the influence of different-type averaging on the kinetic energy spectra for simulations with an initial magnetic field strength of 10 G (panel (a)) and for the observational data (panel (b)). For both the numerical model and the observational data, the averaging shows similar effects, in particular, an increase of the energy spectra slope. This corresponds to a stronger energy filtering of the smaller scales. For the simulated data degraded to the observed spatial resolution, the difference of the energy spectra from the original high-resolution (12.5 km) simulations appears
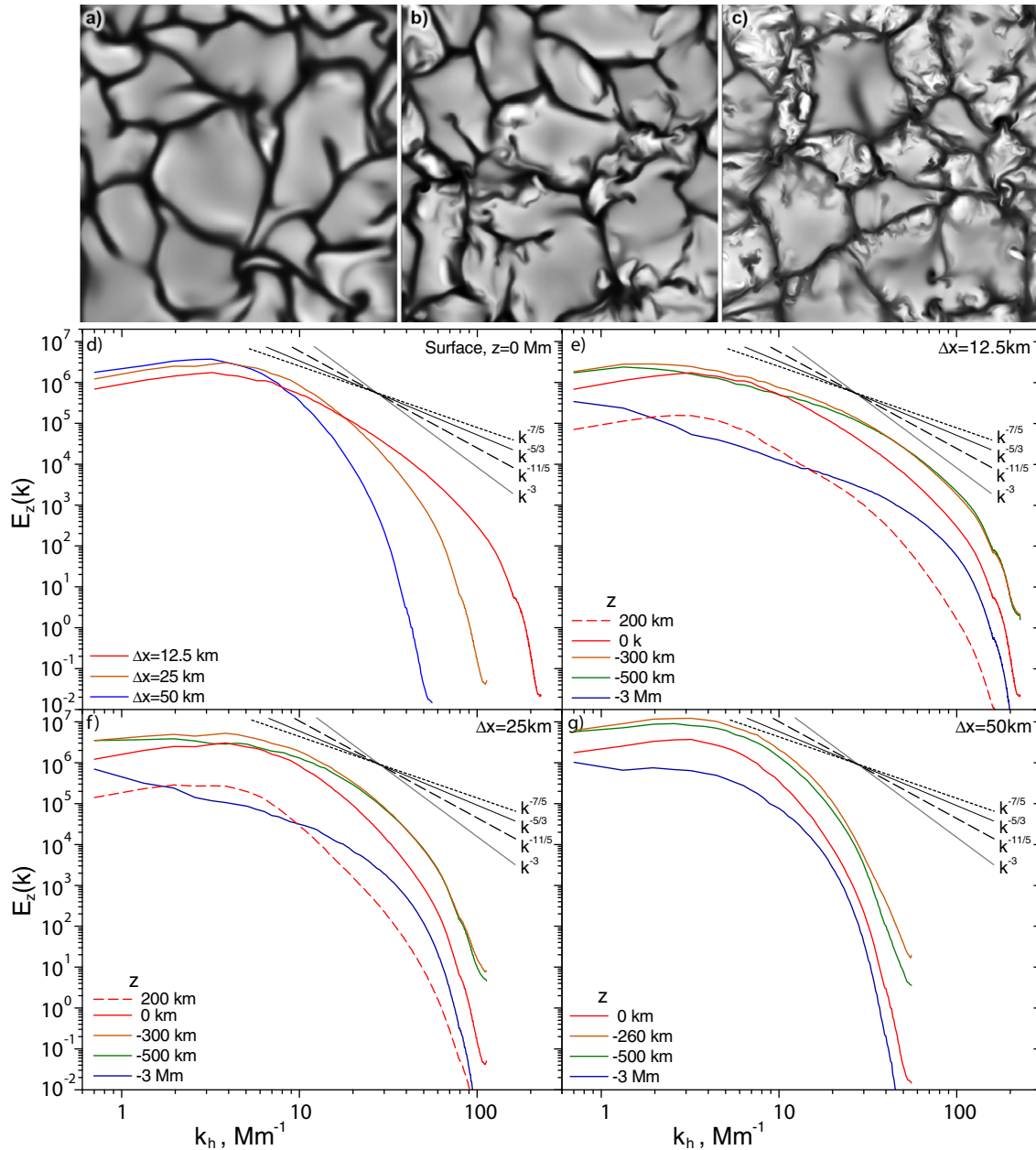
Figure 2. Effect of numerical resolution on the properties of the simulated convection. Top panels show surface snapshots of the vertical velocity for 50 km (a), 25 km (b) and 12.5 km (c) horizontal resolution. Panels (d)–(g) illustrate the effects of different numerical resolutions on the turbulent energy spectra of the vertical velocity: at the photosphere layer (d) and at different locations above and below the photosphere (e)–(g).

Table 1. Parameters of time averaging.

	T_w (s)	T_s (s)	Comments
0	–	–	No averaging
1	20	10	Windows overlapping
2	120	120	Average by bins
3	300	300	Average by bins

only at the smallest resolved scales, due to the turbulent energy cascade cut off at the smaller unresolved scales. In the observational data such an increase of energy also takes place. In the analysis of the solar turbulent dynamics, we would like to keep the maximum amount of the observed signal; therefore we use the ensemble averaging with minimal filtering window properties (case 1, table 1; [23]).

Because we would like to keep most of the signal we use a minimal possible averaging window ($T_w = 20$ s, for 10 s cadence data series) with a corresponding window time shift, $T_s = 10$ s. Thus, in this case, the averaging of two closest in time frames causes the filtration of fluctuations with a scale less than 20 s. Figure 4 illustrates the spectra for the mean (thick curve) and fluctuating (thin) parts of the horizontal velocities for the simulated and observed data obtained by ensemble averaging. Panel (a) shows the energy density spectra obtained from the MHD simulations (with 10 G mean field, red curves). To see the effects of the spatial resolution, we degraded the resolution of the simulated data to the resolution of the observed data (∼50 km, black curves). Because there is no noise in the simulated data, the spectra obtained from the degraded data follow the full resolution
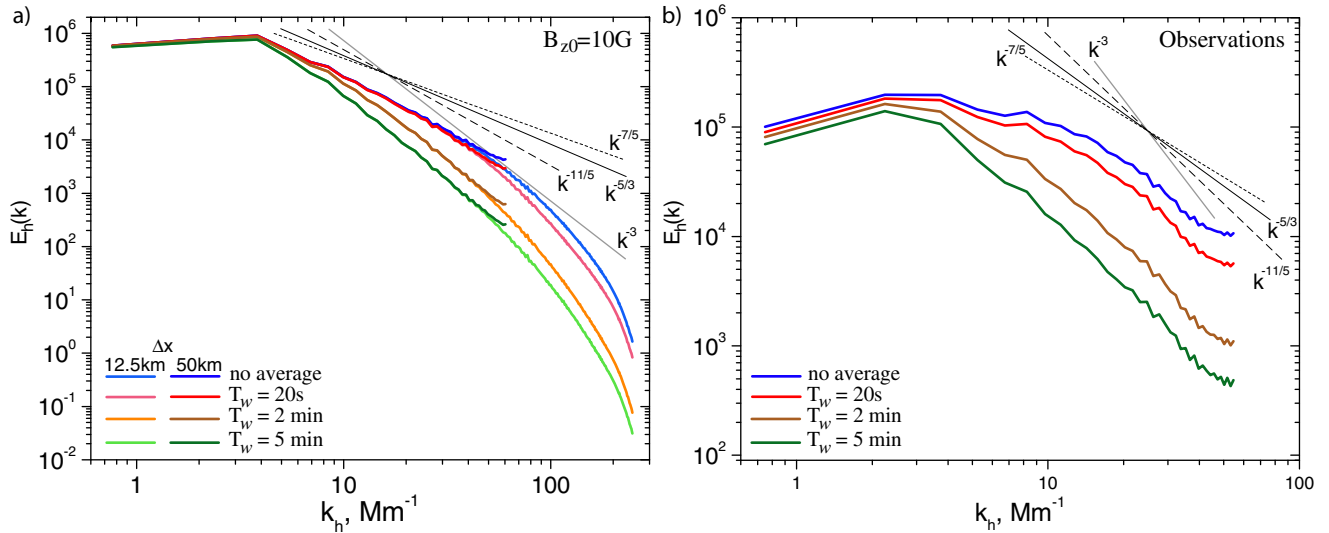
Figure 3. Effect of temporal averaging on the energy spectral density for the horizontal velocity fields in the simulations with an initial vertical field strength of 10 G (a), and the horizontal velocities reconstructed by LCT from the TiO observations at NST/BBSO (b). Panel (a) also shows deviations of the energy spectra for the full resolution of the numerical data (12.5 km) and for the resolution degraded to the observational resolution (50 km). Each panel shows the kinetic energy spectra for the original data set without averaging (blue curves) and for the filtered data sets obtained using the sliding averaging (black and green curves), and 2 and 5 min bin averaging (yellow and red-brown curves).
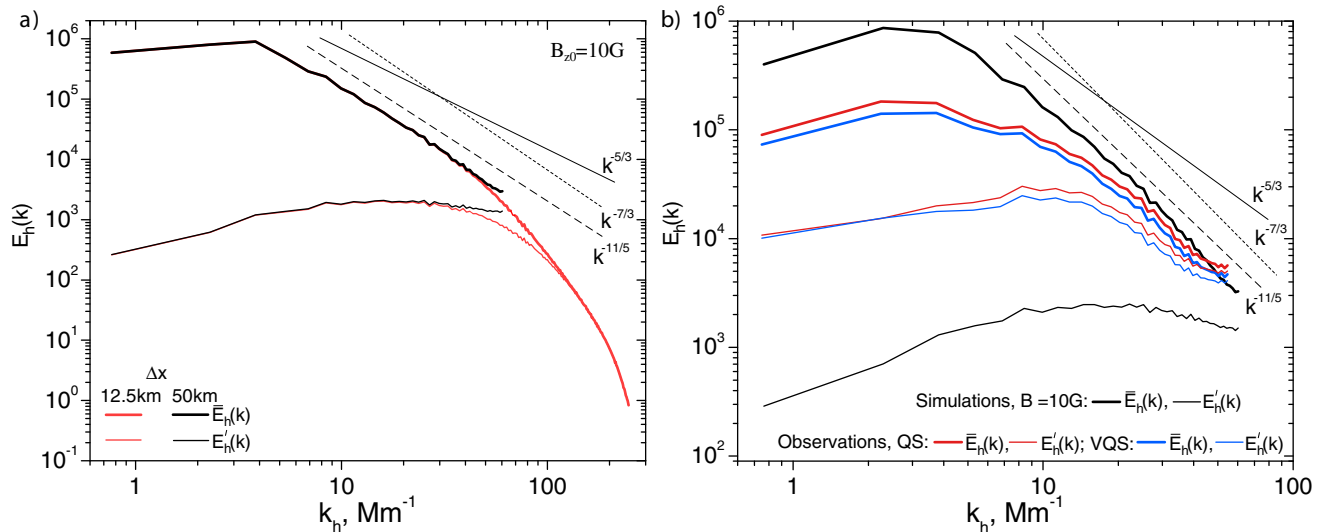

Figure 4. Comparison of the mean and fluctuating parts of the horizontal kinetic energy density obtained by ensemble averaging from simulated and observed data sets (case 1). Panel (a) shows a comparison of the power spectra of the horizontal energy for the mean (thick curves) and fluctuating (thin curves) parts in the high-resolution simulations, $\Delta x = 12.5$ km (red curves), and the simulation data with the degraded spatial resolution ($\Delta x = 50$ km, black curves) for the weak mean initial magnetic field, $B_{z0} = 10$ G. Panel (b) shows the energy density spectra for the degraded simulated data (black curves) and for the quiet-Sun subregion B with magnetic bright points (QS), and for subregion A without magnetic bright points (VQS), indicated in figure 1(a), region A.

spectra on larger scales. The deviations become noticeable only at the smallest resolved scales.

5. Discussion

Investigation of solar convection is of interest from the point of view of the hydrodynamic turbulent properties of the highly stratified medium and also for understanding and characterization the effects of background magnetic fields on the turbulent energy transport between different scales. Recent numerical simulations have shown that the presence of a weak magnetic field can increase the level of nonlinearity

and have different effects at large and small scales due to the increasing inhomogeneity of convective properties and magnetic coupling of plasma motions. In particular, the decreasing of the turbulent kinetic energy at the sub-granular scales in the simulations with magnetic field (black curve, figure 5(a)) can be caused by local suppression of turbulent motions near convective granular edges, where the magnetic field is collapsed into small-scale concentrations of magnetic field ($\sim$1 kG). A recent investigation of quiet-Sun data from the Hinode space mission showed a strong, relatively high contribution of the collapsed field in the magnetic energy density distribution with a maximum at the 80 km
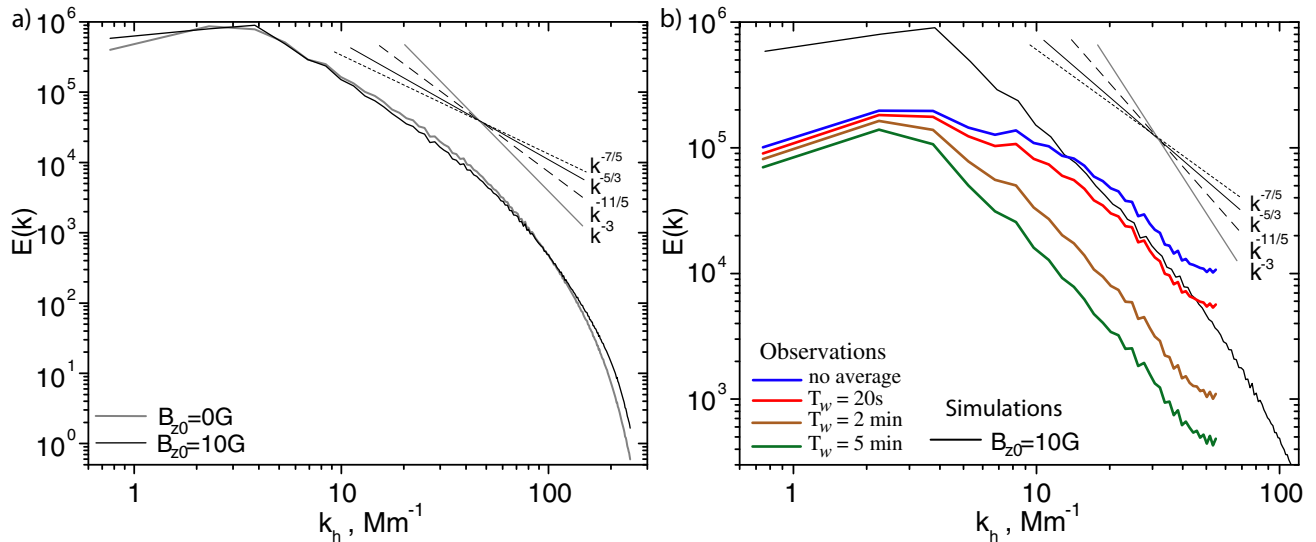
Figure 5. Effect of the background magnetic field (a) and comparison of the kinetic energy spectra for the simulations (with $B_{z0} = 10$ G)
and observations using the horizontal flow velocities reconstructed by the LCT method from the NST/BBSO observations (b).

scale, and the increasing of the magnetic energy density
on granule scales (see the histogram in figure 8 of [27]).
Thus, a comparison of the energy density spectra for the
hydrodynamic and weakly magnetized convection at the solar
surface in figure 5(a) shows a higher kinetic density energy on
scales less than 50 km in the presence of magnetic field, and
the opposite on larger scales. Actually, a similar effect of the
collapsed magnetic flux was found by Stenflo [27], but with
an exponential decrease of the energy density on small scales.
Thus, on small scales (less than 50 km) the increase of the
kinetic energy density reflects an interplay of the collapsing
flux dynamics and probably a small-scale dynamo action.
Perhaps the increase of the kinetic energy density on the small
scales contributes to quasi-periodic flow ejections into the
solar atmosphere by the small-scale vortex tubes as discussed
by Kitiashvili *et al* [15]. This potential relationship needs to
be investigated.

As discussed earlier, data averaging allows us to
filter out noise and makes data sets more homogeneous.
However, increasing the averaging window size can also filter
out short-living features and cause smearing of granules.
Therefore, the averaging effect on the energy spectra, when
most of the energy on the smallest scales is filtered, mostly
leads to a steeper energy spectra slope. Averaging over two
and more minutes makes the slope of the energy spectrum
correspond to the Kolmogorov power law ($k^{-5/3}$; [16]). Such
behavior of the energy spectra reflects the famous in the
turbulence literature Landau's 'Kazan remark' [8], in which
Landau draws attention to the absence of localized small-scale
turbulent fluctuations in the Kolmogorov theory. Only when
such fluctuations are filtered the spectrum becomes of the
Kolmogorov type, as happens in our case.

A comparison of the kinetic energy spectra calculated
from the observational and simulated data sets shows a
higher contribution of flows with small wavenumbers in the
simulations than in the observed data (figure 5(b)). The extra
power in the simulated data on these scales can come from
the geometry of our numerical setup, in which convection is
confined to a box with periodic boundary conditions in lateral

directions, which can cause cutting of the energy transfer to
larger-scale convective modes (e.g. due to inverse cascades).
Also, this deviation can be caused by an underestimation of
the velocity magnitude due to a degrading spatial resolution
of the LCT data analysis procedure.

We have also analyzed effects of the averaging procedure
with different parameters (table 1) on the resulting power
spectra. The ensemble averaging with a minimal size
window ($T_w = 20$ s) and window shift ($T_s = 10$ s, for 10 s
cadence data) filters out most of the noise signal, and
shows good qualitative and quantitative agreement with the
simulated high-resolution data on scales less than ~150 km
(figure 5(b)). In terms of the general properties of the
energy spectra, the time averaging in short bins (2 or
5 min) shows good qualitative agreement with the spectral
profile obtained from the simulated data for all the scales
resolved in the observations. Such good qualitative agreement
in the kinetic energy spectra between the simulations and
filtered observational data can also be due to removal of
additional observational artifacts (such as local uncorrelated
deformations of images and other instrumental effects),
which can have time scales up to several minutes. The
comparison of the energy spectra observed on the small
scales (with wavenumbers larger than 30 Mm^{-1}) with the
spectra calculated from the simulation data degraded to the
observational resolution shows in all cases an increase of the
energy density.

For the investigation of magnetic field effects, we
compared the kinetic energy spectra for two selected regions
(figure 1(a)), one of which (region B) was filled by magnetic
bright points and another (region A) almost lacked these
features. A comparison of the energy spectra of these regions
shows their almost identical behavior, with the total energy
being smaller for region B. Because the difference between
both the spectra is mainly in the energy magnitude, we can
conclude that there was no significant difference in turbulent
dynamics.

Because the background magnetic field is present
on the Sun everywhere, in order to get a more clear

identification of magnetic effects we compare the spectra from the hydrodynamic and weakly magnetized surface turbulence simulations, and can see changes in the energy balance on different scales due to magnetic effects, namely: suppression of turbulent motions on granular scales caused by the accumulation of magnetic field concentrations in the intergranular lanes and increasing of the kinetic energy density for large wavenumbers, probably due to the small-scale dynamo action (figure 5(a)).

6. Summary

We presented a comparison of the kinetic energy spectra of the solar turbulent convection obtained from the observed (NST/BBSO) and simulated ('SolarBox' code) horizontal velocity fields. Our analysis of the energy density spectra for different conditions of convective flows (with and without background magnetic field), different spatial resolutions and data averaging procedures revealed the following properties:

(i) The numerical simulations show good qualitative agreement with the observations in terms of the turbulence properties when the observational data are averaged in 2 min bins. This filtering removes from the observational data noise and relatively long-living (∼1–2 min) artifacts on spatial scales larger than the granule size. In order to reproduce the inertial (Kolmogorov) subrange, it is necessary that the numerical simulations have sufficiently high spatial resolution, 10–25 km per grid step. In this case the transition from the inertial to the dissipative subrange is resolved; the LES turbulence modeling is justified.

(ii) The ensemble averaging method is capable of filtering most of the noise in the data, and provided good qualitative and quantitative agreement between the observed and simulated turbulent spectra on scales 300 km and less (figures 4(b) and 5(b)).

(iii) Different properties of the ensemble averaging (table 1) used for the noise filtering cause changes in the energy spectra, leading in particular to increasing of the slope of the spectra, both in the simulations and the observations (due to stronger filtering on small scales, figure 3).

(iv) Degrading the simulation data to the spatial resolution of observations causes an increase of the energy density on the smallest resolved scales (figures 3 and 4).

(v) The weak background magnetic field changes the energy balance on different scales, namely: (a) suppression of convective motions on larger scales due to the magnetic field structures collapsed in the intergranular lanes and restricting granule motions, and (b) increasing of the kinetic energy density on small scales less than 50 km, probably due to a local small-scale dynamo action (figure 5(a)).

(vi) The energy spectra change qualitatively with depth/height: in the deeper layers, convective turbulence becomes more homogeneous and shows good correspondence to the Kolmogorov power-law turbulent energy cascade (figure 2).

The good agreement between the observed and simulated spectra of the quiet-Sun convection opens up perspectives for a future detailed comparison between numerical models and observations. Our results show the importance of synergy between high-resolution observations and modern realistic-type MHD numerical simulations for understanding complicated turbulent phenomena on the Sun, in the direction of joint data analysis, interpretation and links between observations and models.

Acknowledgment

References

[1] Abramenko V, Yurchyshyn V, Wang H and Goode P R 2001 *Sol. Phys.* **201** 225–40

[2] Abramenko V, Yurchyshyn V, Goode P R and Kilcik A 2010 *Astrophys. J.* **725** L101–5

[3] Abramenko V, Carbone V, Yurchyshyn V, Goode P R, Stein R F, Lepreti F, Capparelli V and Vecchio A 2011 *Astrophys. J.* **743** 133–202

[4] Balarac G, Kosovichev A G, Brugiére O, Wray A A and Mansour N N 2010 *Proc. Summer Program 2010* (*Center for Turbulence Research, Stanford University*) pp 503–12 (arXiv:1010.5759)

[5] Berger T E and Title A M 2001 *Astrophys. J.* **553** 449–69

[6] Brandenburg A, Kemel K, Kleeorin N, Mitra D and Rogachevskii I 2011 *Astrophys. J.* **740** L50–3

[7] Christensen-Dalsgaard J *et al* 1996 *Science* **272** 1286–92

[8] Frisch U 1995 *Turbulence: The Legacy of A N Kolmogorov* (Cambridge: Cambridge University Press)

[9] Germano M, Piomelli U, Moin P and Cabot W H 1991 *Phys. Fluids* **3** 1760–5

[10] Goode P R, Yurchyshyn V, Cao W, Abramenko V, Andic A, Ahn K and Chae J 2010 *Astrophys. J.* **714** L31–5

[11] Goode P R, Coulter R, Gorceix N, Yurchyshyn V and Cao W 2010 *Astron. Nachr.* **331** 620–3

[12] Jacoutot L, Kosovichev A G, Wray A A and Mansour N N 2008 *Astrophys. J.* **682** 1386–91

[13] Kitiashvili I N, Kosovichev A G, Mansour N N and Wray A A 2010 *Astrophys. J.* **719** 307–12

[14] Kitiashvili I N, Kosovichev A G, Mansour N N and Wray A A 2011 *Astrophys. J.* **727** L50–4

[15] Kitiashvili I N, Kosovichev A G, Mansour N N and Wray A A 2012 *Astrophys. J.* **751** L21–7

[16] Kolmogorov A N 1941 *Dokl. Akad. Nauk SSSR* **30** 301–5 Reprinted in Kolmogorov A N 1991 *Proc. R. Soc. Lond.* A **434** 9–13

[17] Manso Sainz R, Martínez González M J and Asensio Ramos A 2011 *Astron. Astrophys.* **531** L9

[18] Matsumoto T and Kitai R 2010 *Astrophys. J.* **716** L19–22

[19] Moin P, Squires K, Cabot W and Lee S 1991 *Phys. Fluids* A **3** 2746–57

[20] Monin A S and Yaglom A M 1963 *Russ. Math. Surveys* **18** 89–109 (in Russian) Monin A S and Yaglom A M 1975 *Statistical Fluid Mechanics* vol 2, ed J Lumley (Cambridge, MA: MIT Press) (translated)

[21] November L J and Simon G W 1988 *Astrophys. J.* **333** 427–42

[22] Rieutord M, Roudier T, Rincon F, Malherbe J-M, Meunier N, Berger T and Frank Z 2010 *Astron. Astrophys.* **512** A4

[23] Reynolds O 1895 *Phil. Trans. R. Soc.* **186** 123–64
[24] Rogers F J, Swenson F J and Iglesias C A 1996 *Astrophys. J.* **456** 902–8
[25] Smagorinsky J 1963 *Mon. Weather Rev.* **93** 99–164
[26] Stein R F and Nordlund Å 1998 *Astrophys. J.* **499** 914–33
[27] Stenflo O 2012 *Astron. Astrophys.* **541** A17

[28] Strous L H, Scharmer G, Tarbell T D, Title A M and Zwaan C 1996 *Astron. Astrophys.* **306** 947–59
[29] Wöger F, von der Lühe O and Reardon K 2008 *Astron. Astrophys.* **448** 375–81
[30] Yurchyshyn V B, Goode P R, Abramenko V I and Steiner O 2011 *Astrophys. J.* **736** L35–40